Effect of the local morphology in the field emission properties of conducting polymer surfaces

2013 J. Phys.: Condens. Matter 25 285106

(http://iopscience.iop.org/0953-8984/25/28/285106)

J. Phys.: Condens. Matter **25** (2013) 285106 (9pp) doi:10.1088/0953-8984/25/28/285106

Effect of the local morphology in the field emission properties of conducting polymer surfaces

T A de Assis[1,2,3], R M Benito[2], J C Losada[2], R F S Andrade[3], J G V Miranda[3], Nara C de Souza[4], C M C de Castilho[5,6], F de B Mota[5] and F Borondo[1,7]

[1] Departamento de Química, Universidad Autónoma de Madrid, Cantoblanco, E-28049 Madrid, Spain
[2] Grupo de Sistemas Complejos, Departamento de Física y Mecánica, ETSI Agrónomos, Universidad Politécnica de Madrid, Ciudad Universitaria, E-28040 Madrid, Spain
[3] Instituto de Física, Universidade Federal da Bahia, Campus Universitário da Federação, Rua Barão de Jeremoabo s/n, 40170-115, Salvador, BA, Brazil
[4] Grupo de Materiais Nanoestruturados, Campus Universitário do Araguaia Universidade Federal de Mato Grosso, 78698-000, Barra do Garças, Mato Grosso, Brazil
[5] Grupo de Física de Superfícies e Materiais, Instituto de Física, Universidade Federal da Bahia, Campus Universitário da Federação, Rua Barão de Jeremoabo s/n, 40170-115, Salvador, BA, Brazil
[6] Instituto Nacional de Ciência e Tecnologia em Energia e Ambiente, Universidade Federal da Bahia, Campus Universitário da Federação, Rua Barão de Jeremoabo s/n, 40170-115, Salvador, BA, Brazil
[7] Instituto de Ciencias Matemáticas (ICMAT), Universidad Autónoma de Madrid, Cantoblanco, E-28049 Madrid, Spain

E-mail: t.albuquerque@uam.es, rosamaria.benito@upm.es, juancarlos.losada@upm.es, randrade@ufba.br, ncsouza@ufmt.br, caio@ufba.br, fbmota@ufba.br and f.borondo@uam.es

Received 13 March 2013, in final form 29 May 2013
Published 26 June 2013
Online at stacks.iop.org/JPhysCM/25/285106

Abstract
In this work, we present systematic theoretical evidence of a relationship between the point local roughness exponent (PLRE) (which quantifies the heterogeneity of an irregular surface) and the cold field emission properties (indicated by the local current density and the macroscopic current density) of real polyaniline (PANI) surfaces, considered nowadays as very good candidates in the design of field emission devices. The latter are obtained from atomic force microscopy data. The electric field and potential are calculated in a region bounded by the rough PANI surface and a distant plane, both boundaries held at distinct potential values. We numerically solve Laplace's equation subject to appropriate Dirichlet's condition. Our results show that local roughness reveals the presence of specific sharp emitting spots with a smooth geometry, which are the main ones responsible (but not the only) for the emission efficiency of such surfaces for larger deposition times. Moreover, we have found, with a proper choice of a scale interval encompassing the experimentally measurable average grain length, a highly structured dependence of local current density on PLRE, considering different ticks of PANI surfaces.

(Some figures may appear in colour only in the online journal)

1. Introduction

Conducting polymers (CPs) such as polyaniline (PANI) are considered nowadays as very good candidates [1] in the design of field emission (FE) devices [2], for example as nanotubes [3, 4], and chemical sensors [5].

In this context, understanding the surface characteristics, such as the local morphology, is very important, and indeed the existence of specific emitting spots is known to critically determine the electronic emission properties [6]. This is particularly relevant in view of an eventual control of

the surface growth process when a FE device with some predetermined specifications is required. As an example, we may quote the distribution of FE centers on a fractal surface model that was studied in a previous work [7]. Despite the fact that surface roughness starts at early growth stages at an atomic scale, the validity of such models is supported by the fact that growth dynamics in actual systems, e.g. CPs, lead to nm or even μm roughnesses [8]. We concluded in [7] that the global fractal dimension of the surface is directly related to the effective field amplification factor. In this respect there is a puzzling question that we want to address in this paper: Is there any basic universal measure relating the extremely low macroscopic threshold fields observed in the FE properties of some conducting materials to their surface geometry?

Nowadays, there exist very powerful techniques to directly determine surface structures with a great degree of accuracy at very detailed length scales. Among them, atomic force microscopy (AFM) deserves a special mention. Interesting information provided by AFM includes the size and density of highly packed small protrusions formed on the surface, and the variations of its morphology with the preparation conditions. This fact can identify, for instance, the optimum annealing time where a remarkably low FE threshold can be observed [9]. The local morphological characteristics of the kind of surfaces that we are considering here are ultimately a consequence of, or develop in, the surface growing process.

Surface growth has been a fascinating topic in statistical mechanics for many years, showing that scale invariance and universality are not restricted to equilibrium conditions [10]. The global interface roughness $\Omega_{\mathrm{G}}(L, t)$, usually estimated by the width or by the standard deviation of the local surface height $z(\vec{r}, t)$ over a length scale L (system size), is found to follow the so-called normal Family–Vicsek scaling law [11]

$$\Omega_{\mathrm{G}}(L, t) \sim t^{\beta} F\left(Lt^{-1/\mathbf{z}}\right) \sim \begin{cases} L^{\alpha} & \text{for } L \ll L_{\mathrm{c}}, \\ t^{\beta} & \text{for } L \gg L_{\mathrm{c}}, \end{cases} \quad (1)$$

α and β being two global characteristic exponents, $\mathbf{z} \equiv \alpha/\beta$, and $L_{\mathrm{c}} \sim t^{1/\mathbf{z}}$ is a crossover length. However, in actual experimental situations related to the growth of molecular thin films, effects such as adatom diffusion, step-edge barriers, or grain boundaries lead to the emergence of anomalous roughening, i.e. different scalings for the global and local surface fluctuations. In such cases the relation (1) does not hold.

In a seminal paper [12], Kardar, Parisi, and Zhang (KPZ) proposed an equation to model the interface growth through stochastic evolution, which captures the essential aspects of many interesting situations. The comparison of KPZ predictions with experiments has often been based on estimations of global exponents α and β. More recently, a detailed analysis has become possible by a direct comparison between the measured height distributions [13, 14] and the Tracy–Widom (TW) [15–17] and Halpin-Healy [18] distributions, respectively the distributions followed by the KPZ systems on 1D and 2D substrates [18, 19]. Actually, it has been argued in [20] that the growth of PANI surfaces may follow the KPZ theory.

The purpose of this paper, which is based on experimental atomic height actual data on CP surfaces obtained by AFM, is twofold. First, we report measurements of the point local roughness exponents (PLRE) associated with surface coarse grained patches. Second, we present an electronic emission model establishing the local emitting properties of these surfaces. With respect to the experimental data it should be stated that they are restricted to only three different thickness values, for which we succeeded in providing a consistent picture of the PANI growth mechanism. The small number of samples, however, prevented the possibility of presenting a more accurate statistical study. Accordingly, we use PLRE which can be accurately defined with the set of data at hand. The combination of the above mentioned results indicates that the PLRE constitutes a potentially useful geometrical measure associating the surfaces heterogeneity with their electronic FE current density properties. The PLRE takes into account not only the geometry of a particular region of the material, but also that of the corresponding neighborhood, which substantially affects quantities such as the characteristic barrier field and thus the characteristic field enhancement factor. Our results, based on experimental data, constitute a theoretically sound explanation that clarifies the relations between roughness of a substrate/film and several electronic field emission properties. These puzzling questions, which were quoted in the second paragraph of this introduction, have been addressed in a number of previous studies.

2. Local morphological analysis of CP surfaces

The study that we present here is based on actual experimental height measurements, $z(\vec{r}, t)$, for three conducting PANI surfaces of different thickness [20]. The samples were obtained by growing films using the Langmuir–Blodgett technique [21], which allows a precise control of the molecular architecture, improving the stability of the electric properties when PANI gets mixed with other materials.

AFM images (512 × 512 pixels) on a scan window of $5 \times 5\ \mu\mathrm{m}^2$ were taken with a Digital Instruments Multimode SPM Nanoscope IIIa set in tapping mode and under ambient conditions at room temperature. This tapping mode was selected, instead of the contact mode, since it is less damaging to the surfaces under investigation [22]. It allows for a smaller amount of transferred energy, as the tip does not exert a significant lateral force on the surface. It is known that distortions in the image may occur due to the finite size of the AFM tip [23–25]. However, we assume that in our measurements these distortions did not affect the interpretation in our comparative analysis.

Distinct morphologies result from stopping the growth process at different fixed times. In our case, surfaces consisting of 1, 11, and, 21 deposited monolayers were obtained. In figure 1 we present the scaled height defined by $\xi(x, y) \equiv [(z(x, y) - \langle z \rangle)/\sigma]$ considering a range ($x \in [1, 3]\ \mu\mathrm{m}$; $y \in [1, 3]\ \mu\mathrm{m}$) of the PANI surfaces consisting of (a) 1, (b) 11 and (c) 21 monolayers (labeled CP1, CP11, and CP21). Here, $\langle z \rangle$ is the average value of $z(x, y)$ in the window with area L^2 (L denote the total system size), and

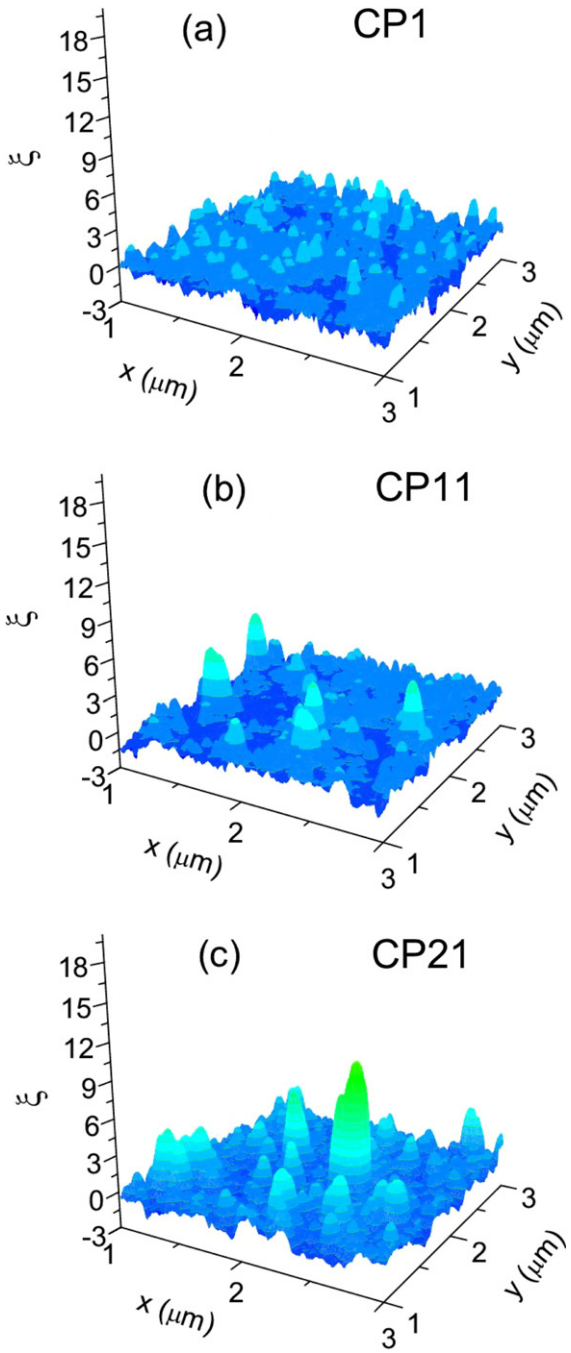

Figure 1. Scaled height $\xi(x, y)$ for PANI surfaces consisting of (a) 1, (b) 11 and (c) 21 monolayers (CP1, CP11, CP21), in the range $x \in [1, 3]$ μm and $y \in [1, 3]$ μm. Here, $\xi(x, y) \equiv [(z(x, y) - \langle z \rangle)/\sigma]$, where $\langle z \rangle$ is the average value of $z(x, y)$ in the window with area L^2 and σ corresponds to the standard deviation of surface fluctuations.

σ corresponds to standard deviation of surface fluctuations. From these measurements, the local roughness $\Omega(\ell)$ can be calculated in the following way

$$\Omega(\ell) = \frac{1}{N_\ell} \sum_{\epsilon=1}^{N_\ell} \left\{ \left[\frac{1}{m_\ell} \sum_{k \in \ell} [z(x_k, y_k) - \langle z \rangle_\ell]^2 \right] \right\}^{1/2}, \quad (2)$$

where N_ℓ indicates the total number of windows of size ℓ, m_ℓ is the number of points within a window of size ℓ, $z(x_k, y_k)$ represents the regularly spaced height of the surface, while $\langle z \rangle_\ell$ is the average value of $z(x_k, y_k)$ in the kth window.

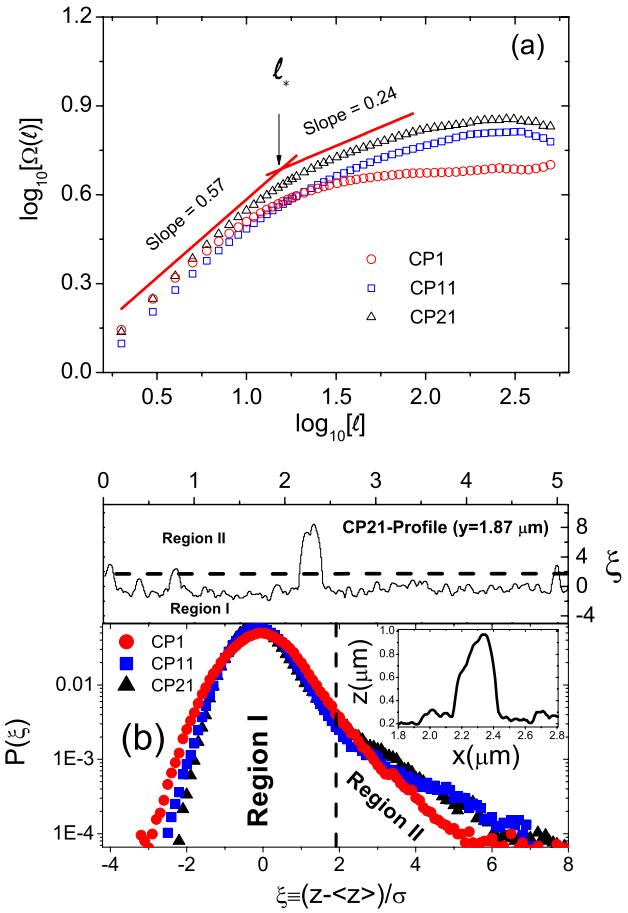

Figure 2. (a) Scaling properties of PANI surfaces consisting of 1, 11 and 21 layers (CP1, CP11, CP21). The roughness slope for CP21 shows a crossover at $\ell_* \approx 165$ nm. (b) Normalized scaled height distributions $P(\xi)$ for CP1, CP11, CP21. In the inset, a blow up of the right tail (in log-linear scale to enlarge the difference between CP11 and CP21 experimental points). The dashed line separates two regions: (I)—corresponding to less protruding structures and (II)—corresponding to typical protruding grain structure. In the inset, a typical irregular protruding grain profile from CP21 surface. Above the main panel, we show a profile (obtained from CP21 for $y = 1.37$ μm). The dashed black line corresponds to the value of ξ indicated in the inset.

The corresponding results are shown in figure 2(a). As it can be seen, $\Omega_{CP1} < \Omega_{CP11} < \Omega_{CP21}$ for $\ell = L$, thus indicating that the number of individual polymer grains increases with the number of deposited layers. More information about the grains can be obtained from the data. Indeed, if we consider the CP21 surface, two distinct scaling regimes are observed in the $\log_{10}\{\Omega(\ell)\} \times \log_{10}\{\ell\}$ plots before the final saturation region is reached. Namely, one in the interval ~20–160 nm, which corresponds to ℓ smaller than the mean size of the granular structures, and another one for ~170–600 nm, characterizing fluctuations in height differences at a scale larger than individual grains. To help identifying these two different regimes, in figure 2(a) we draw vertically displaced straight lines obtained in a least square fitting procedure for $\log_{10}\{\Omega(\ell)\}$ of the CP21 surface. In the

case of the CP1 surface the effect is less obvious since the density of spots is significantly smaller. Although we can identify an interval ∼30–90 nm inside the grains is very difficult to discern between the two scaling regimes before saturation. For CP11 we identify the scale interval inside and outside the grains as ∼30–130 nm and ∼140–600 nm. Also at the smallest scales we see that the local surface roughness depends on the number of deposited layers. This allow us to identify an anomalous scaling behavior in the polymer thin film growth. These features are similar to some results reported in [26], in which anomalous scaling in polymer thin film growth surfaces was verified.

For the CP21 surface, the limiting local roughness exponents, i.e. slopes for the two regimes, are $\alpha^{(1)}_{\mathrm{CP21}} = 0.57 \pm 0.01 > \alpha^{(2)}_{\mathrm{CP21}} = 0.24 \pm 0.01$, respectively (for CP11 surface we obtain $\alpha^{(1)}_{\mathrm{CP11}} = 0.49 \pm 0.01 > \alpha^{(2)}_{\mathrm{CP11}} = 0.19 \pm 0.01$). These values indicate that the structure inside the grains ($\ell < \ell_*$) is smoother than that resulting from the assembly of different individual grains ($\ell > \ell_*$). The actual value of the crossover length gives an estimation of the average grain size; in our case, $\ell_* \approx 165$ nm for the CP21 surface and $\ell_* \approx 135$ nm for CP11 surface. It should be remarked that the values of local roughness exponents, $\alpha^{(1)}_{\mathrm{CP21}}$ (or $\alpha^{(1)}_{\mathrm{CP11}}$) are different from those found in numerical simulations for $2 + 1$ growth systems [27] considering semi-elliptical, conical or pyramidal grain shapes. This results can be related to more irregular shapes of real grains in our surfaces. Moreover, a comparison between the local exponents ($\alpha^{(1)}$) obtained by CP11 and CP21 surfaces shows a weak dependence of this magnitude on the shape of the grains.

Another interesting point is that the values of $\alpha^{(2)}$ are different from those that characterize the dynamics in the KPZ class of universality in $2 + 1$ surface growth. In fact, in [28], has been found in Kardar–Parisi–Zhang growth, the possibility of obtain very different values of $\alpha^{(2)}$, ranging from 0.4 for the films with smoothest surfaces to values in the range $0.1 \lesssim \alpha^{(2)} \lesssim 0.2$ for systems with large cliffs separating the grains. This latter result is consistent with those obtained in our surfaces despite our results indicating anomalous scaling.

Some interesting behaviors are found, which are unveiled in the more detailed data analysis presented in figure 2(b) (along with a representative image revealing details of the typical irregular grain of CP21 surface). Here, the experimental scaled height histogram, $P(\xi)$ (where $\xi \equiv (z - \langle z \rangle)/\sigma$), for the CP1, CP11 and CP21 surfaces are shown. In CP11 and CP21 surfaces we can see two more pronounced regions: the first one corresponding to smaller fluctuations (see Region I defined in figure 2(b) above), and the second one corresponding to more protruding grains (see Region II defined in figure 2(b) above). As will be discussed later, this kind of behavior in Region II (more slowly decaying in right tail) is responsible for an enhanced electronic field emission current density from the deviating centers, which can give special emitting properties to the surface if adequately controlled during the growth process.

3. Point local morphological analysis of CP surfaces

As we have seen, the local roughness exponent (LRE) can characterize the local morphology of all disordered surfaces, and identify different scaling regimes. However, LRE just provides an indication of the surface heterogeneity, making difficult the identification of clear morphologic differences in surfaces sharing the same value of the LRE. For this reason, we will consider instead a *point local* version, PLRE, which is able to characterize the heterogeneity around each individual surface point. This measure is conveniently assessed by averaging the height fluctuations, $\Omega(\ell)$, in square patches of different sizes around all points of the surfaces [29].

Indeed, we evaluate the PLRE by measuring $\Omega(\ell)$, defined by equation (2), at all points of the cathode surface in a square window (patch) of the total window with a defined length of size $2\ell_{\mathrm{max}}$. In this procedure, the window is chosen so that $\ell < \ell_{\mathrm{max}}$, taking into account scales inside the grains. Thus, an important computational detail in this procedure is the definition of the scale interval $[\ell_{\mathrm{min}}, \ell_{\mathrm{max}}]$. For the sake of clarity, we include this information in our notation by calling the PLRE as $\alpha_{[\ell_{\mathrm{min}}, \ell_{\mathrm{max}}]}$. In our case, we based the choice of these bounds considering the average grain length determined by the crossover ℓ_* defined in figure 2(a) and discussed in section 2.

Therefore, it is wise to adopt a range of $[\ell_{\mathrm{min}}, \ell_{\mathrm{max}}] \equiv [30, \ell_*]$ nm, and evaluate the PLRE within this range that takes into account the grain features. We remark that this measure (PLRE) is more reliable than that based on an interval that takes into account scales spanning structures inside and outside the grain, as will be discussed in the next section. In this way, the lower bound of the interval (30 nm) lies within the range of the emitting structures, while the upper bound corresponds to the typical average length of grainy structures, which depends therefore on the number of deposited monolayers. The actual values indicated in figure 2(a) illustrate the above discussion and provide typical values occurring in our experimental data.

The corresponding $\alpha_{[30,90]}$, $\alpha_{[30,130]}$ and $\alpha_{[30,160]}$ maps, for CP1, CP11 and CP21 surfaces respectively, are shown in figure 3. It can be seen that the results are clearly correlated with the elevation map for the same surface presented in figure 1, the thickest areas showing higher values of PLRE. We remark that the upper bound for PLRE evaluation in the CP1 surface ensures the inclusion of the typical length scales inside the largest (isolated) grains (see discussion in section 2). On the other hand, a careful examination of figure 3 reveals that, as more layers are deposited, the most protruding grains have a PRLE very close to 1 (see the profiles at the top and right part of figures 3(a)–(c)). This indicates two features: (i) the grain surface is very smooth as compared with the large height differences in the borders; (ii) the grains are sharpest. Moreover, for CP21 surface our results indicate that the PLRE becomes lower in the rest of the sample, typically $\alpha_{[30,160]} \sim 0.30$–$0.80$. For the CP11 surface we can see grains with PLRE slightly below 1 (and thus less sharp than the grains of the CP21 surface) and the rest of sample presents values of $\alpha_{[30,130]} \sim 0.35$–$0.80$. Finally, and

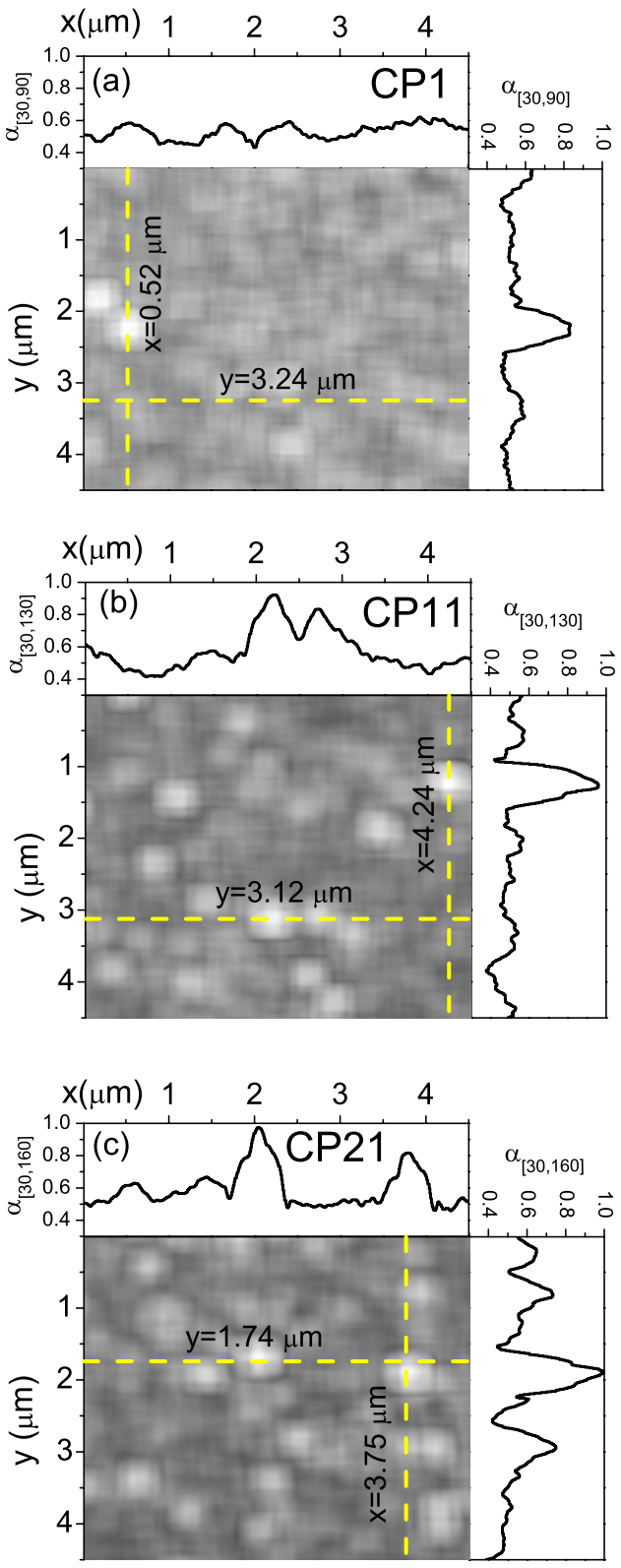

Figure 3. PLRE map and profiles corresponding to the dashed line which cross the surface for (a) CP1, (b) CP11 and (c) CP21. The corresponding scale intervals in which the PLRE were evaluated are [30, 90] nm, [30, 130] nm and [30, 160] nm respectively.

interestingly enough, the mainly grainy structures present in the CP1 surface yield $\alpha_{[30,90]}$ close to 0.80, suggesting the possibility of sharp rounded granular surface (not sharper than

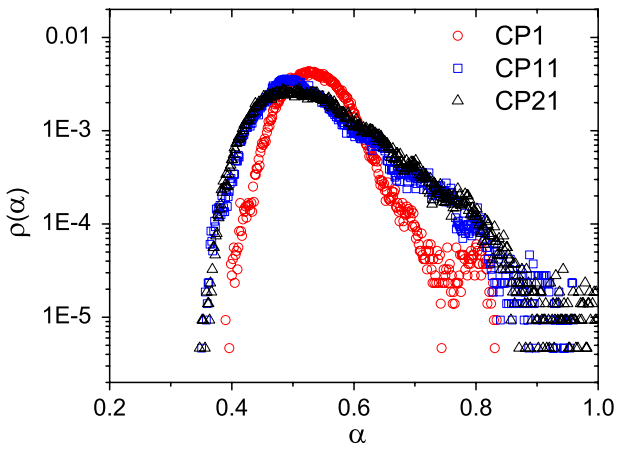

Figure 4. PLRE distribution, $\rho(\alpha)$, evaluated from the maps shown in figure 3.

CP11 and CP21 surfaces). The rest of sample presents values of $\alpha_{[30,90]} \sim 0.40$–$0.70$.

To further analyze these data we present in the figure 4 a histogram with the PLRE distribution (frequencies $\rho(\alpha)$) considering the same maps in figure 3. We can see that, as the film thickness increases (from CP1, to CP11, and to CP21) the PLRE distribution widens. This is a consequence of the increase in the density of grains, which implies an increment of the global surface roughness Ω_L, that changes from 50.24, to 60.18, and to 67.70 nm. Similarly to the discussion for the model surface in [7], it can be expected that the previous results should have a clear influence on the FE properties of our CP surfaces.

4. Field emission analysis

To investigate this point we have theoretically computed the electric field strengths F over the surface of our CP cathode surfaces [$z = z(x, y)$]. Actually, the electric field was calculated by taking the gradient of equipotential surfaces Φ_ϱ, staying as close as possible to the position of the surface. For this purpose, we first numerically integrate the corresponding Laplace's equation in the region limited by a CP cathode and a flat parallel anode located far away from it, using Liebmann's method [7, 30]. The CP surface and the distant plane are maintained at constant potential values of $\Phi = 0$ and Φ^{A}, respectively. From these results, the local electronic current density $J_L(z)$ was obtained by using the standard simplified Dyke–Dolan–Fowler–Nordheim-type equation:

$$J_L(z) = a\varphi^{-1}F^2 \exp\left[-v(f)b\varphi^{3/2}/F\right], \qquad (3)$$

where a and b are the first and second Fowler–Nordheim constants respectively, $v(f) \approx 1 - f + (1/6)f\ln(f)$ [31], and $f = F/F_{\mathrm{R}}$ is the scaled barrier field for a Schottky–Nordheim barrier of unreduced height φ (for our conducting surfaces $\varphi \approx 4.8$ eV). The term F_{R} corresponds to the 'reference field' needed to reduce to zero a Schottky–Nordheim barrier of height equal to the local work function and can be written as $F_{\mathrm{R}} = c^{-2}\varphi$, where c is the Schottky constant. From

this, a parameter η can be defined as $\eta = bc^2\varphi^{-1/2}$. In this way, introducing the Forbes approximation for $v(f)$, the exponential factor in equation (3) can be expanded as

$$\exp\left[-v(f)b\varphi^{3/2}/F\right] \approx e^{\eta}\left[\frac{F}{F_R}\right]\exp\left[-b\varphi^{3/2}/F\right]. \quad (4)$$

Then, using equations (3) and (4), the local electronic current density is given by [31, 32]

$$J_L(z) = a\varphi^{-1}e^{\eta}(F_R)^{\eta/6}F^{(2-\eta/6)}\exp\left[-b\varphi^{3/2}/F\right]. \quad (5)$$

At this point it is interesting to define some useful quantities for a better understanding of experimental details. A quantity that experimentalists actually measure is the so-called 'macroscopic current density' J_M, defined in our case by:

$$J_M = i/A_M \approx \frac{\sum_p J_L(z_p)\Delta A_p}{A_M}, \quad (6)$$

where i is the total emission current, A_M is the total 'substrate footprint', and the sum is taken over the whole surface area of the emitter. Furthermore, the values of $J_L(z_p)$ are given by equation (5). In our calculations, the space is covered by a discretized cubic lattice with unit volume $\Delta x \times \Delta y \times \Delta z$. We use an approximation in which each point of the cathode surface represents a particular lateral location on the emitter surface. With these arguments, equation (6) can be written as

$$J_M \approx \frac{\sum_p J_L(z_p)\Delta x_p \Delta y_p}{(N_x-1)\Delta x \times (N_y-1)\Delta y} = \frac{\sum_p J_L(z_p)}{(N_x-1)\times(N_y-1)}, \quad (7)$$

where N_x and N_y represent the number of points defining the CP surfaces in the x and y directions respectively. In equation (7) we consider $\Delta x_1\Delta y_1 = \cdots = \Delta x_{N_x}\Delta y_{N_y} = \Delta x\Delta y$. In some reported cases, the term $\sum_p J_L(z_p)$ is called J_T, $(N_x-1)\times(N_y-1)$ is called M and the ratio given by equation (7) is called $\langle J\rangle$ (see for instance [30]). Actually, J_M was calculated by integrating over an equipotential surface (ϱ) slightly above a 'step-like' CP surface defined by $\Phi_\varrho = 10^{-2}$ V.

The corresponding results for our surfaces, for which $\eta \approx 4.49$, are shown in the Fowler–Nordheim plot (FNP) of figure 5(a). As can be seen, the macroscopic current density, J_M, increases with the number of deposited layers, a tendency that saturates for the thickest considered surface, CP21. This result can be interpreted as a consequence of the widening in the PLRE distribution, implying in an increase in the density of grains, as discussed in the previous section (see figure 4). These effects explain the behavior of J_M, which is observed in the corresponding FNPs. The slope S_{Φ^A} of a FNP drawn as function of the reciprocal of the cathode–anode potential difference Φ^A can be written as:

$$S_{\Phi^A} = -\sigma b^{3/2}(d/\gamma_C), \quad (8)$$

where σ is a slope correction factor, d is the mean cathode–anode separation, and the characteristic field

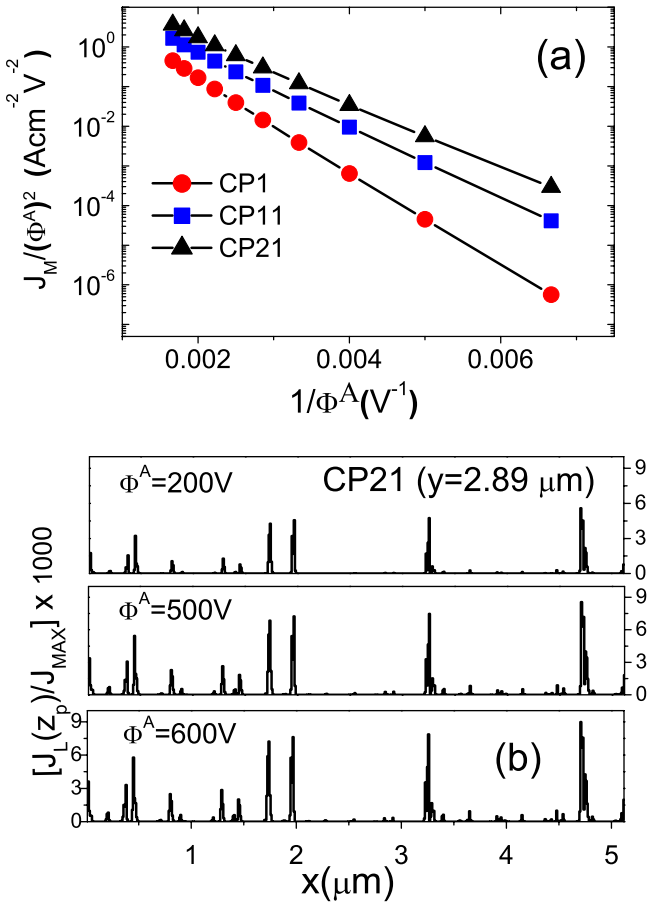

Figure 5. (a) Theoretically predicted Fowler–Nordheim plots for the CP surfaces. (b) Normalized local current density profiles (at $y = 2.89$ μm—see the text for more details) considering the CP21 surface, for $\Phi^A = 200$, 500 and 600 V.

enhancement factor (characteristic FEF) γ_C is defined by:

$$\gamma_C = F_C/F_M = F_C d/\Phi^A. \quad (9)$$

Here, F_C is a characteristic barrier field and F_M [$= \Phi^A/d$] is the macroscopic field. For convenience, the field F_C can be identified as the highest local field in the cathode surface, and is usually found at the sharpest part of the surface. It is clear from the equations (8) and (9) that the higher the characteristic FEF γ_C, then the lower in magnitude will be the FNP slope S_{Φ^A}. This trend is visible in figure 5(a) and reflects, in the case of CP1 surface, not only the lowest density of grains existing in the corresponding surface, but also the fact that these are less protruding. Indeed, this information could also have been guessed from the higher values of the PLRE (close to unity) for surfaces of thicker films, which leads to a higher FEF [33]. Finally, the saturation observed in the FNPs, as the number of deposited layers increases, is an indication of the stabilization taking place in the grain density, something that allows the optimization of the macroscopic electronic current density, J_M.

Now, we address our main point, which is to show the clear relationship existing between the PLRE and the FE properties in our CP surfaces. We compute these dependences for all surfaces studied here: CP1, CP11 and CP21, at a

fixed value of the anode potential, $\Phi^{A} = 600$ V, a choice that guarantees that the artificial emission current surface where the height of which is equal to the normalized current density produced by the corresponding site at the emission surface, $J_L(z_p)/J_{MAX}$, has reached its asymptotic configuration. This fact is shown in figure 5(b), where we present the profiles $J_L(z_p)/J_{MAX}$ considering the CP21 surface (at $y = 2.89$ μm—this value defines the profile $z(x, 2.89\ \mu\text{m})$, similar to that defined in the caption of figure 3 for the PLRE map.), for $\Phi^{A} = 200$, 500 and 600 V from top to bottom. We can clearly see that the morphology of the profiles for $\Phi^{A} = 500$ and 600 V are very similar, suggesting an asymptotic configuration.

In figure 6, we show the results for the normalized local electronic current density, $J_L(z_p)/J_{MAX}$, as a function of the PLRE value for our CP surfaces. In other words, we consider here the values of the electronic current density at each point, $J_L(z_p)$, as a function of the local roughness exponent at the same point. An important aspect of the developed procedure is the determination of the best accurate interval for the PLRE evaluation $[\ell_{min}, \ell_{max}]$, as illustrated in the insets of figure 6. When this interval is restricted to be inside the grain scale (∼[30, 90] nm for CP1), (∼[30, 130] nm for CP11) and (∼[30, 170] nm for CP21) the errors are smaller as compared to situation considering a value of ℓ_{max} that includes structures outside the grains, for instance $\ell_{max} =$ 300 nm. When $[\ell_{min}, \ell_{max}] \sim [180, 300]$ nm; a condition that characterizes the region outside the typical grain size, the calculation takes into account the effect of grain assemblies. In this case (not shown in figure 6), the use of the [180, 300] nm range for the PLRE evaluation leads to a blurred picture which masks the existence of the surface grains. Then, with a choice of a scale interval that encompasses the average grain length, it is possible to observe a highly structured dependence of $J_L(z_p)$ on PLRE, which will be used for the further discussion of our results.

In this way, it can be seen in both surfaces CP11 and CP21 that the largest values of $J_L(z_p)/J_{MAX}$ are found in those regions where $\alpha_{[30,130]} \approx 1$ and $\alpha_{[30,160]} \approx 1$, respectively in agreement with the results in figure 4, for the dependence of the PLRE distribution with the number of deposited layers. Moreover, the data corresponding to the CP1 surface present abrupt changes, which are related to lower density of grains. We can notice in the corresponding plots the sudden emergence of a sharp valley, i.e., a well defined region along the PLRE axis where the emitted current has very small values. For $\alpha_{[30,90]}$, this region is observed for PLRE ∼0.71–0.78. As mentioned before, the density of pronounced protruding granular structures is very small for the CP1 surface. Since these grains are relatively far apart from each other, the electrical interaction between them is quite small. Thus, a larger charge density is expected at the corresponding tips (which corresponds to $\alpha_{[30,90]} \sim 0.80$). Consequently, the valleys around them exhibit a smaller emitting capacity. Indeed, we have observed in the analysis of our theoretical calculations that the PLRE values for such curves at the base of the spots are in the interval 0.78–0.71. On the other hand, values of the PLRE in the interval (0.38, 0.71) are

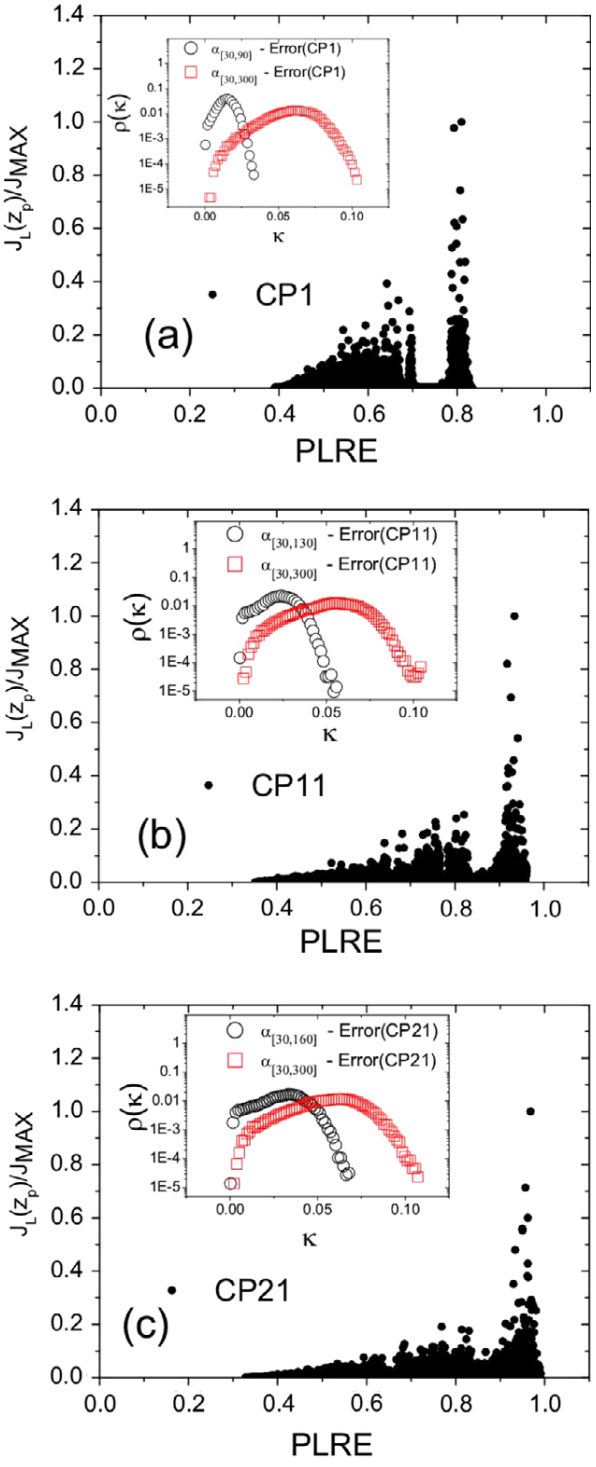

Figure 6. Normalized local electronic current density calculated at the anode potential $\Phi^{A} = 600$ V, as a function of the PLRE for (a) CP1, (b) CP11 and (c) CP21. The PLRE was evaluated for the scale interval inside of the grains, [30, 90] nm (a), [30, 130] nm (b), and [30, 160] nm (c). The corresponding insets show the errors on the PLRE estimation, considering the length intervals limited by the grain size (black circles) and length intervals that include structures inside and outside the grains (red squares).

typical of the regions constituted by less protruding grains and smaller fluctuations (see figure 3), where the electric interaction appears between smaller peaks, which constitute

the majority of the CP surface. This explains why the emitting regions can include even those sites at the hill sides.

The results for the CP11 and CP21 surfaces are similar, with a peak of current density at $\alpha_{[30,130]} \sim \alpha_{[30,160]} \sim 1.0$. This result reflects the combined effect of more protruding grains within a smoother geometry. This behavior is consistent with the fact that the magnitudes discussed here tend to saturate as the number of deposited layers increases. In the case of $J_L(z_p)/J_{\mathrm{MAX}}$, this is due to the fact that, in the thick layer limit, the number of comparatively large spots is reduced by the growth dynamics. These results indicate that, when the number of monolayers in the surface is small, the emitted current is subject to large local fluctuations that depend on the PLRE, but the total emitted current is small. When more layers are added to the sample, the total current is enhanced. Such an increase of the emitting current comes concomitantly with a larger number of emitting spots with PLRE $\sim$ 0.5–0.7, as well as with the emergence of a few spots with PLRE $\sim$ 0.9–1.0. This confirms the especial importance of the Region II defined in figure 2(b). This interesting feature of our CP surfaces can lead to reduction of the screening effect more efficiently than the other regions of the rough emitter surface, in agreement with recent experimental and theoretical studies with ZnO nanorod arrays [34].

Finally we stress that our study, including the theoretically investigation of the real geometry of materials, can provide new insights concerning the results obtained experimentally on the field emission properties of promising materials that present roughness dependent of scale. The PLRE encompasses not only the geometry of a particular region of the material, but also the corresponding neighborhood. As we know, it substantially affects the characteristic barrier field F_{C}, and then the characteristic FEF. Moreover, this tool leads to a geometric interpretation in terms of PRLE definition, showing that the local current density varies strongly with location on the surface of the complete emitter. Nevertheless, it will assume its highest values for the strongly emitting regions at the tips of pointed structures.

5. Conclusions

Summarizing, this work unveils a number of coupled effects, due to the transient heterogeneity in CP surface deposits. They include the form of the height probability distribution, point local roughness exponent, and surface emitting properties. By analyzing AFM experimental data, we have studied the local morphology of PANI surfaces. The two different expected regimes have been identified. Also, we have found an anomalous scale in our systems, and a local roughness exponent for length scales larger than that of the grains smaller than that predicted for the $2 + 1$ KPZ equation.

Our results show an important effect of the number of monolayers in the corresponding emitted current density. For a small number of monolayers, the system is subject to large local fluctuations that depend on the local PLRE, but the total emitted current is small. When more layers are added to the sample, the total current is enhanced for two different reasons: the overall increase of emitting spots with intermediate PLRE values, and the formation of a few coherent structures with PLRE near to 1.0. This suggests that the corresponding total emission becomes more uniformly distributed despite the existence of large size structures.

Moreover, a clear relation between the surface heterogeneities and field emission properties has been reported using the PLRE measurements. This interesting result can explain in systematic manner the particular threshold field/film thickness relationship observed and reported in many experimental situations.

Finally, and more specifically, we have shown that PLRE can be a promising tool to characterize the control growth process of a surface device. It can be easily evaluated by considering the average length of grains extracted from experimental AFM measurements. The devised practical application may be adequate if an enhanced emitting property related to surface heterogeneity is desired for an specific application. We expect that our results may be helpful for the interpretation of previous or future works that include thin film deposition for applications in field emission devices, where the real geometry exhibits a essential role.

Acknowledgments

This work has been supported by MINECO (Spain) under projects MTM2012-39101 and ICMAT Severo Ochoa SEV-2011-0087, AECI (Spain), CAPES (Brazil), CNPq, INCT-SC (Brazil) under grant 306052/2007-5, and PRONEX-FAPESB grant 0006/2009 (Brazil).

References

[1] Nair R, Premlal B, Das A and Sood A 2009 *Solid State Commun.* **149** 150
[2] Lai G, Li Z, Cheng L and Peng J 2006 *J. Mater. Sci. Technol.* **22** 677
[3] Poa C H P *et al* 2005 *J. Appl. Phys.* **97** 114308
[4] Patil S S *et al* 2011 *J. Electrochem. Soc.* **158** 63
[5] Janata J and Josowics M 2002 *Nature Mater.* **2** 19
[6] Zou Q, Wang M Z and Hatta A 2009 *Plasma Devices Operat.* **17** 82
[7] de Assis T A, Borondo F, Benito R M and Andrade R F S 2008 *Phys. Rev.* B **78** 235427
[8] Liu S, Montazami R, Liu Y, Jain V, Lin M, Heflin J R and Zhang Q M 2009 *Appl. Phys. Lett.* **95** 023505
[9] Chen D, Wong S P, Cheung W Y and Xu J B 2003 *Solid State Commun.* **435** 435
[10] Barabasi A L and Stanley H E 1995 *Fractal Concepts in Surface Growth* (Cambridge: Cambridge University Press)
[11] Family F and Vicsek T 1985 *J. Phys. A: Math. Gen.* **18** 75
[12] Kardar M, Parisi G and Zhang Y C 1986 *Phys. Rev. Lett.* **56** 889
[13] Takeuchi K A and Sano M 2010 *Phys. Rev. Lett.* **104** 230601
[14] Takeuchi K A, Sano M, Sasamoto T and Spohn H 2011 *Sci. Rep.* **1** 34
[15] Sasamoto T and Spohn H 2010 *Phys. Rev. Lett.* **104** 230602
[16] Dean D S and Majumdar S N 2006 *Phys. Rev. Lett.* **97** 160201
[17] Kriegerbauer T and Krug J 2010 *J. Phys. A: Math. Gen.* **43** 403001
[18] Halpin-Healy T 2012 *Phys. Rev. Lett.* **109** 170602
[19] Calabrese P and Doussal P L 2011 *Phys. Rev. Lett.* **106** 250603
[20] de Souza N C *et al* 2007 *Nanotechnology* **18** 075713
[21] Bal J K, Kundu S and Hazra S 2010 *Phys. Rev.* B **81** 045404

[22] de Souza N C *et al* 2006 *J. Colloid Interface Sci.* **297** 546
[23] Santos N C *et al* 1998 *Biophys. J.* **75** 1869
[24] Waner M J, Gilchrist M, Schindler M and Dantus M 1998 *J. Phys. Chem.* B **102** 1649
[25] Lechenault F, Pallares G, George M, Rountree C, Bouchaud E and Ciccotti C 2010 *Phys. Rev. Lett.* **104** 025502
[26] Son S-W, Ha M and Jeong H 2009 *J. Stat. Mech.* 02031
[27] Oliveira T J and Reis F D A A 2011 *Phys. Rev.* E **83** 041608
[28] Oliveira T J and Reis F D A A 2007 *J. Appl. Phys.* **101** 063507
[29] Vázquez E V, Miranda J G V and González A P 2005 *Ecol. Modelling* **182** 337
[30] de Assis T A, Borondo F, de Castilho C M C, Mota F B and Benito R M 2009 *J. Phys. D: Appl. Phys.* **42** 195303
[31] Forbes R G and Deane J H B 2007 *Proc. R. Soc.* A **463** 2907
[32] Forbes R G 2008 *Appl. Phys. Lett.* **92** 193105
[33] Forbes R G 2012 *Nanotechnology* **23** 095706
[34] Pan N, Xue H, Yu M, Cui X, Wang X, Hou J G, Huang J and Deng S Z 2010 *Nanotechnology* **21** 225707